Geochemical Journal, Vol. 37, pp. 199 to 216, 2003

Geochemistry of water discharges from the Libiola mine, Italy

LUIGI MARINI,* GIUSEPPE SALDI, FRANCESCO CIPOLLI,
GIULIO OTTONELLO and MARINO VETUSCHI ZUCCOLINI

Department for the Study of the Territory & Its Resources, Genoa University,
Corso Europa 26, 16132 Genoa, Italy

(*Received April 2, 2002; Accepted October 28, 2002*)

Two distinct groups of mine waters are found at Libiola. They are red acid waters (pH 2.4–2.8) and blue neutral waters (pH 7.0–7.5), based on the color of the precipitating solid phases. Few occurrences have characteristics intermediate between those of red waters and blue waters. The irreversible mass exchanges taking place during interaction of meteoric waters with mine-waste materials and addition of local groundwaters to acid mine waters were simulated by means of the software package EQ3/6. Results of these simulations were compared with the analytical data of mine waters through activity plots, showing the fields of stability of dominant sulfate, hydroxide, and carbonate minerals. The activity plots and the bimodal distribution of pH in mine waters indicate that the main process governing the chemistry of the mine waters of Libiola is variable interaction of meteoric waters with mine-spoil materials. Mixing between local groundwaters and acid mine waters plays a minor role, if any.

INTRODUCTION

The acid waters of the Libiola mine, with pH as low as 2.4, are a typical example of acid mine drainage (AMD). The primary cause of AMD is the oxidative dissolution of pyrite, whose mechanisms and rates have been thoroughly investigated during the last 40 years (e.g., Garrels and Thompson, 1960; Singer and Stumm, 1970; Lowson, 1982; Nordstrom, 1982a; McKibben and Barnes, 1986; Moses *et al*., 1987; Nicholson *et al*., 1988; Moses and Herman, 1991; Williamson and Rimstidt, 1994). The rate of the process depends on several factors, including pH, Eh, surface area and morphology of pyrite, oxidants taking part to the reactions, presence or absence of aerobic S- and Fe-oxidizing bacteria, etc. Pyrite oxidation driven by atmospheric O_2 initially produces H^+, SO_4^{2-}, and Fe^{2+}. Ferrous ion can be further oxidized to Fe^{3+}, which either precipitates as ferric hydroxide (pH > 3.5) or remains in the aqueous solution (pH < 3.5; Nordstrom, 1982a). In the latter case, pyrite oxidation is prevailingly driven by Fe^{3+} (Singer and Stumm, 1970; Moses *et al*., 1987). Unfortunately, at these low pH values, an Fe-oxidizing bacterium, *Thiobacillus ferrooxidans*, speeds up the O_2-driven oxidation of Fe^{2+} to Fe^{3+} by a factor greater than 10^6 (Singer and Stumm, 1970). Under these conditions the overall process, i.e., Fe^{3+} reduction to Fe^{2+} by pyrite plus oxidation of Fe^{2+} to Fe^{3+} by atmospheric O_2, is very fast. In mine wastes, where pyrite has generally become fine-grained due to crushing, acid production is particularly effective, especially above the water table, where oxidation rates are enhanced by bacterial catalysis (Langmuir, 1997). Acid waters usually acquire high concentrations of metals through interaction with metal-rich mine wastes (e.g., Appelo and Postma, 1996).

Although the high concentrations of metals and the high acidity of the waters discharging from

*Corresponding author (e-mail: lmarini@dipteris.unige.it)

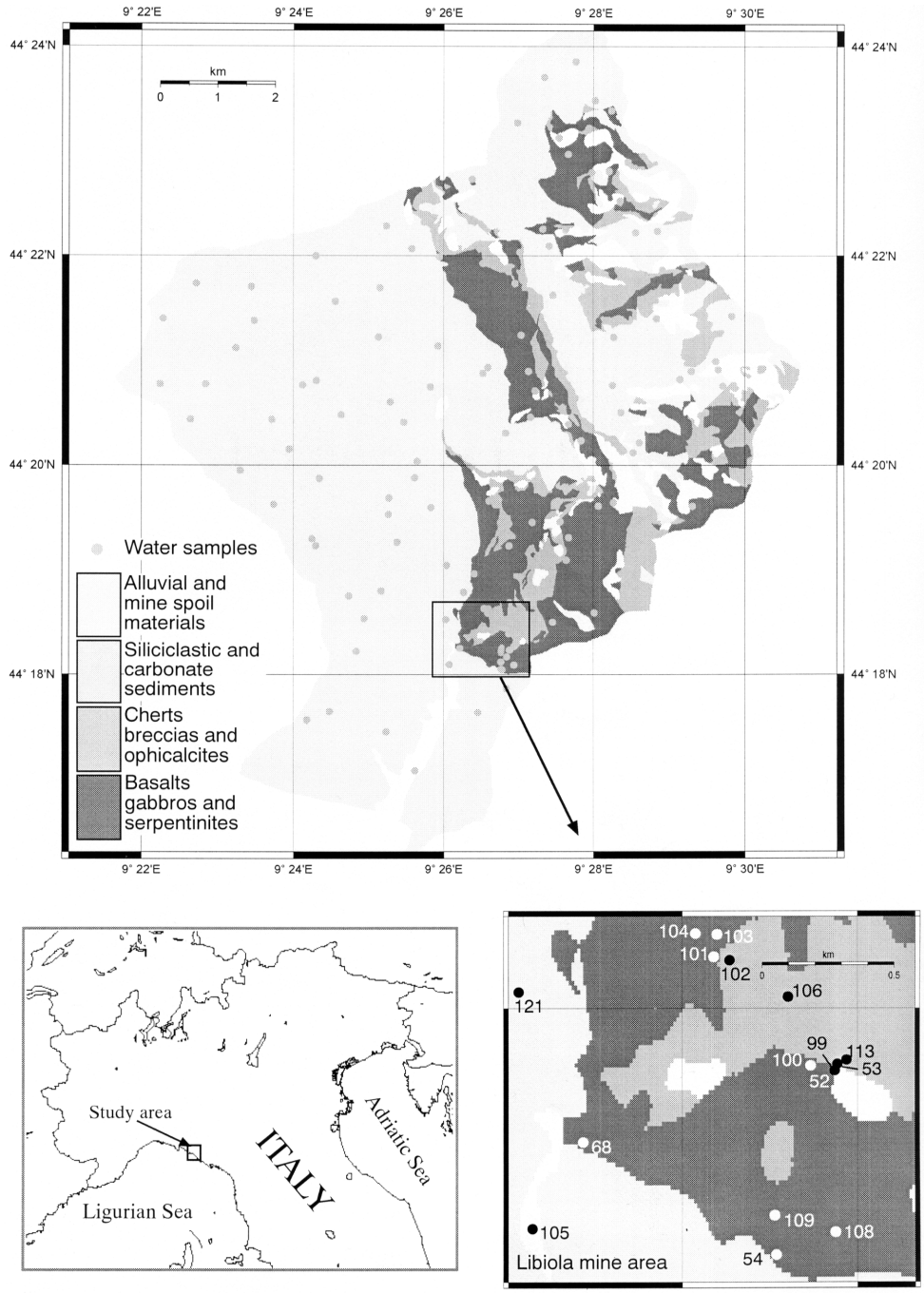

Fig. 1. Simplified geological map of the Graveglia valley and the Gromolo basin (from Decandia and Elter, 1972 and Abbate et al., 1980), also showing the location of the sampled waters.

the abandoned mine site of Libiola is partly mitigated by neutralization through water-rock interaction and/or dilution, these waters have a remarkable impact on the surrounding environments (Dubuis *et al*., 1998; Derron, 1999; Dinelli *et al*., 2001; Cortecci *et al*., 2001), similar to what has been observed around many sulfide and coal mines throughout the world (Evangelou, 1995). Development of remediation strategies to mitigate these environmental damages (e.g., application of limestone or organic wastes, application of bactericides, establishment of wetland technologies, application of clay liners, plastic liners, or asphalt, use of microencapsulation (coating) methodologies, etc., Evangelou, 1995) demands first that we understand the processes of mobilization, transport, and sequestration of relevant chemical components occurring in the mine site. This can be elucidated through reaction path modeling, a powerful geochemical technique proposed by Helgeson (1968), who worked out the equations needed to compute the irreversible mass transfers among minerals, aqueous species, and gases.

This paper investigates the geochemical processes controlling the fate of relevant chemical components in the mine drainage from Libiola by comparing the theoretical results of reaction path modeling with a set of analytical data comprising both available observations and newly acquired ones.

Geological Background

The geological formations cropping out in the study area (Fig. 1) have been ascribed to the Bracco-Val Graveglia and Monte Gottero (or Val Lavagna) tectonic units (Decandia and Elter, 1972; Abbate *et al*., 1980). The Monte Gottero unit includes the flyschoid sequences of Upper Cretaceous–Paleocene age belonging to the Gottero sandstones and the Val Lavagna Formation. This unit is superimposed on the Bracco-Val Graveglia unit, which is made up of ophiolitic rocks (peridotites variably affected by serpentinization, gabbros, and basaltic dykes) and the related volcano-sedimentary cover rocks of Jurassic–Upper Cretaceous age. These include ophiolitic breccias, basaltic lavas, and pelagic sediments (cherts, micritic limestones, and claystones).

The Ore Deposit of Libiola

The sulfide ore deposit of Libiola is located into the Gromolo basin, ~8 km NE of Sestri Levante (Fig. 1). It is one of the numerous mineralizations associated with the Apennine ophiolites (Ferrario, 1973; Brigo and Ferrario, 1974). These ore deposits were originally generated by convective circulation of seawater through hot rocks at spreading ridges and underwent subsequent metamorphic and tectonic processes during the Apennine orogenesis (Bonatti *et al*., 1976). Today, this interpretation is substantiated by the data acquired from over 100 seafloor venting sites, discharging metal-rich fluids at temperatures ≤405°C (Scott, 1997 and references therein).

The Libiola ore deposit was made up of massive lens-shaped bodies concordant with pillow basalts and disseminated mineralizations, comprised of small aggregates of sulfides, either filling vescicular cavities or concordant with the textures of pillows. The serpentinites tectonically overlying the basalts also host small irregular mineralized veins (Brigo and Ferrario, 1974).

The primary mineralogic association is pyrite and chalcopyrite, with subordinate sphalerite, pyrrhotite, marcasite, hematite, mackinawite, magnetite, cubanite, and gold. Scarce gangue minerals include quartz and carbonates (Bertolani, 1952; Ferrario and Garuti, 1980).

The Libiola mine was already active in the Bronze Age, but its intensive exploitation began in 1864 and maximum production was attained in the beginning of the 20th century (Galli and Penco, 1996). For instance, 28×10^6 kg of pyrite and 7.5×10^6 kg of Cu minerals were extracted in 1905, when over 700 workers were employed. In more recent years, the main ore body, with an areal extension of 85 m × 60 m and a maximum thickness of ~250 m, was mined through 21 levels of tunnels, extending from 72 to 321 m above msl (acronym of mean sea level), as well as by shafts

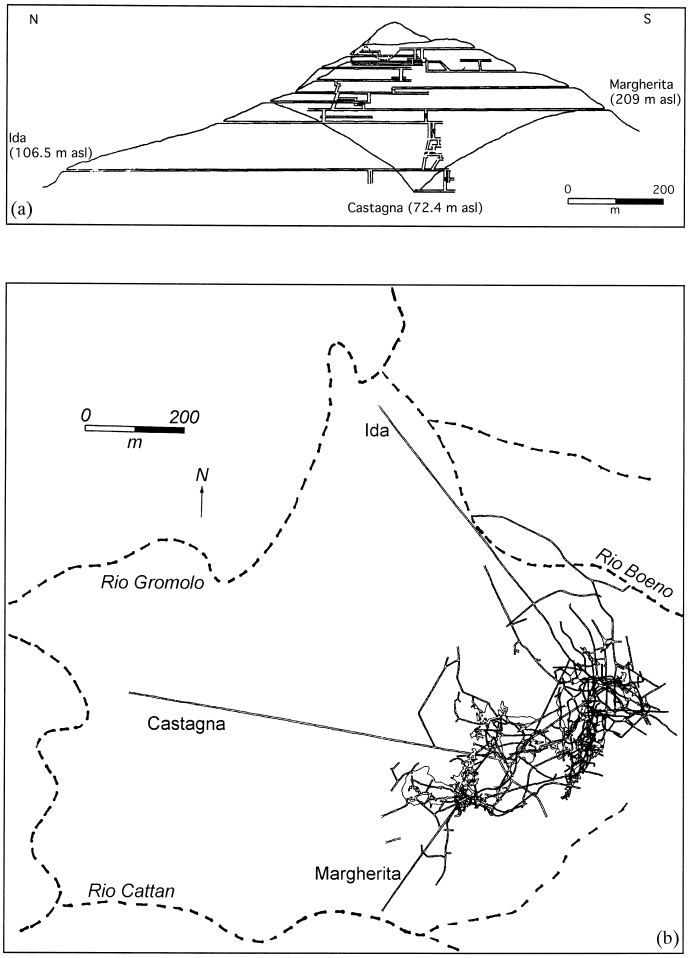

Fig. 2. (a) Projected cross section and (b) planimetry of the Libiola mine.

and open pits (Fig. 2). Mining ended in 1962. Based on the documents available at the Mining District of Carrara, a total of ~6×10^8 kg of pyrite, with Cu contents of 1–2%, and ~4×10^8 kg of Cu minerals, with an average grade of 5–10% Cu, were extracted from the Libiola mine from 1878 to 1954 (Galli and Penco, 1996). In addition, Cu was obtained from acid waters by treatment with Fe shavings.

This long-lasting mining activity left a considerable amount of wastes as heaps without vegetation covering a total area of ~500,000 m^2. The mine wastes are poorly sorted, either sterile or mineralized rock fragments, chiefly serpentinites and basalts, and secondary mineral phases produced by weathering, mainly Fe oxyhydroxides brown-reddish-orange in color. Locally these Fe oxyhydroxides form a hard surface layer which favors high-angle stratification of waste piles.

AVAILABLE AND NEWLY ACQUIRED DATA

The acid and neutral waters discharging from the Libiola mine area, as well as local stream waters, were the subject of investigations, mainly concentrating on their chemistry (Dubuis *et al.*, 1998; Derron, 1999; Dinelli *et al.*, 2001; Cortecci *et al.*, 2001; Dinelli and Tateo, 2002). Some δD and δ^{18}O values of rainwaters, surface waters, and groundwaters were also reported by Dubuis *et al.*

Table 1. Concentrations of chemical constituents and other relevant data for the waters of the Libiola mine area sampled in this work (nd = not detected). Samples 68, 168, 101, 52, 152, 99, 100, 109, 54, and 154 are from tunnels; sample 53 is an ephemeral discharge; samples 102, 103, 104, 105, and 113 are from streams.

Code	Name	Type or notes	Sampling date	*T* °C	Eh mV	pH	Alkalinity ppm HCO_3	SO_4 ppm	Cl ppm	NO_3 ppm
68	Castagna	red water	May 2000	13.9	601	2.53	nd	9570	7.0	26.5
168	Castagna	red water	June 2000	14.5	621	2.48	nd	9050	9.8	10.7
101	Ida	red water	June 2000	14.3	611	2.52	nd	4480	11.5	22.7
52	Weirs	red water	May 2000	16.8	605	2.43	nd	5690	7.1	0.9
152	Weirs	red water	June 2000	16.2	625	2.40	nd	5880	10.3	1.7
53		inter. water	May 2000	12.3	457	3.28	nd	201	6.7	0.6
99	Edifici	inter. water	June 2000	14.6	437	3.52	nd	2120	2.0	14.3
100	Della Strada	inter. water	June 2000	12.9	514	3.28	nd	2610	12.0	10.0
109		inter. water	June 2000	15.1	143	7.62	54.9	665	9.6	1.3
54	Margherita	blu water	May 2000	15.4	195	7.02	43.3	1410	10.7	5.2
154	Margherita	blu water	June 2000	15.6	156	7.54	74.7	1430	9.1	0.6
106		spring water	June 2000	13.8	97	7.41	235	111	7.6	0.6
103	Rio Gromolo	upstream	June 2000	20.4	98	8.43	188	8.3	8.5	1.7
104	Rio Gromolo	downstream	June 2000	20.3	161	6.88	80.9	260	14.7	0.8
105	Rio Gromolo	downstream	June 2000	21.4	150	6.86	18.3	403	7.4	0.7
102	Rio Boeno	downstream	June 2000	18.1	169	7.95	68.6	343	8.4	2.8
113	Rio Boeno	downstream	June 2000	15.1	170	7.05	97.6	133	5.2	0.7

Code	Na ppm	K ppm	Mg ppm	Ca ppm	Al ppm	Fe ppm	Cu ppm	Zn ppm	Mn ppm	SiO_2 ppm
68	33.0	0.1	1090	165	59.5	1000	23.4	31.4	8.1	128
168	27.1	0.3	936	172	203	843	177	50.8	7.8	155
101	24.3	1.0	479	238	5.4	309	69.2	28.0	3.9	116
52	20.0	0.5	671	385	23.8	378	84.8	28.6	6.4	212
152	16.4	0.3	632	445	97.1	356	118	32.1	8.0	230
53	2.3	0.2	22.7	18.2	0.06	0.6	0.35	0.084	0.013	80.2
99	6.8	1.1	314	171	33.4	1.3	39.8	14.1	2.8	159
100	11.3	1.3	311	320	32.9	2.6	29.0	19.6	4.4	134
109	4.9	0.6	114	103	0.004	0.004	0.21	1.70	0.053	48.4
54	13.8	2.8	238	146	0.039	0.21	1.95	6.59	1.1	59.7
154	12.8	2.6	226	219	0.007	0.21	0.64	3.3	0.87	57.4
106	4.3	0.1	66.7	12.8	0.004	0.008	0.012	0.015	0.001	59.1
103	3.6	0.2	28.4	19.8	0.001	0.014	0.006	0.002	nd	42.7
104	4.6	0.2	60.9	39.5	0.017	0.009	0.17	0.64	0.15	42.7
105	7.5	0.5	70.4	53.6	0.012	0.022	0.17	0.59	0.19	32.7
102	4.6	0.4	72.5	48.2	0.037	0.077	0.36	0.92	0.14	74.3
113	3.2	0.1	34.9	13.9	nd	0.005	0.015	0.037	nd	67.3

(1998), whereas a few $\delta^{34}S$ values of dissolved sulfate and metal sulfides were obtained by Cortecci *et al*. (2001). Mine-spoil materials and stream sediments from mined and unmined areas were collected and analysed both for mineralogy (XRD) and chemistry (XRF) by Dinelli *et al*. (2001). The solid phases precipitated by mine waters at their surface outlet were analysed by XRF and FT-IR spectrometry by Derron (1999), and by XRF, XRD, FT-IR spectrometry, TG, DTG, and DTA by Dinelli and Tateo (2002).

After a critical review of the existing data, we decided to complement them with the following investigations.

(1) Two hydrogeochemical surveys of the waters discharging from the Libiola mine area, one at the end of a rainy period (May 2000) and another during a relatively dry period (June 2000). Ten samples from seven different tunnels were thus collected, plus one sample from an ephemeral discharge, which was active during the rainy period only. Three stream water samples were also collected from the Rio Gromolo, upstream and downstream of the mine discharges, and two samples were taken from its tributary passing close to the mine site, the Rio Boeno.

(2) A hydrogeochemical survey of the spring waters of the Gromolo basin and of the adjacent Graveglia valley, for a total of 114 sampling sites.

(3) The collection and analysis of three samples of mine-spoil materials, to check previous data.

Sampling and analytical techniques of waters and mine-spoil materials are summarized below. Relevant results for the waters of the Libiola mine area are reported in Table 1. Other data are available upon request to the corresponding author (LM).

Waters

Outlet temperature, pH, Eh, TDS, and dissolved O_2 (where possible) were measured at each sampling site by means of portable instruments. pH-meter was calibrated on site against two pH buffers with nominal pH values of 4 and 7. Eh was measured with a Pt electrode and values were corrected against the ZoBell's solution (Nordstrom, 1977). The analytical uncertainties for pH and Eh are ~0.05 units and ~30 mV, respectively. Water was filtered through 0.45 μm membranes of cellulose acetate and a portion was stored without further treatments. A separate portion of filtered water was acidified, by addition of concentrated HNO_3 (1 ml in 200 ml), and stored. New polyethylene containers were used.

Within a few days after collection, all water samples were analysed by the AMGA laboratories of Genova as follows. (1) Na, K, Mg, Ca, Ba, B, Al, Cr, Mn, Ni, Cu, Zn, and Pb by ICP-MS; (2) Fe by AAS with graphite furnace; (3) Cl, SO_4, and NO_3 by IC; (4) SiO_2, NO_2, and NH_4 by visible spectrophotometry; (5) total alkalinity by acidimetric titration. Acid mine waters were also analysed for Ag, As, Au, Bi, Cd, Co, Mo, V, Sb, Se, and Sn by ICP-MS. Short-term analytical precision (repeatability) is better than 3% for ICP-MS analyses and alkalinity, ~5% for AAS and IC determinations, and 5–10% for visible spectrophotometry. Concentrations of Fe^{3+} and Fe^{2+} were computed from total Fe and Eh by means of the computer code EQ3NR (Wolery, 1992).

Mine-spoil materials

In the field, mine-spoil materials coming from the uppermost horizon (0–20 cm) were sieved retaining the fine-grained fraction (<3 mm), which was stored in plastic bags. In the laboratory, samples were dried in air at 40°C, pulverized in a mill with agate balls and stored in new polyethylene containers. Samples were analyzed by the ACME Analytical Laboratories Ltd., Vancouver, Canada (ISO 9002 Accredited Co.) as follows.

(1) Approximately 0.2 g of each sample were fused with 1.5 g of $LiBO_2$ and the obtained glass was dissolved in 100 ml of 5% HNO_3. This solution was analyzed by ICP for Si, Al, Fe, Mg, Ca, Na, K, Ti, P, Mn, Cr, Ba, Ni, Sr, Zr, Y.

(2) Approximately 15 g of each sample was digested with 90 ml of aqua regia at 95°C for 1 hour and the solution was diluted to 300 ml. Co, Th, V were determined directly by ICP; Mo, Cu, Pb, Zn, Ag, As, Cd, Bi, Hg, were extracted with methyl isobutyl ketone (MIBK) and analysed by ICP; Au was also extracted with MIBK and determined through GF/AA.

(3) On a separate sample portion, total S and C were analysed by IR spectrometry after volatilization of all S and C compounds through heating at temperatures >1650°C.

WATER CHEMISTRY

The chemical composition of the waters sampled in the study area is investigated in terms of relative Cl, SO_4 and HCO_3 concentrations (Fig. 3a) and relative Na + K, Ca and Mg contents (Fig.

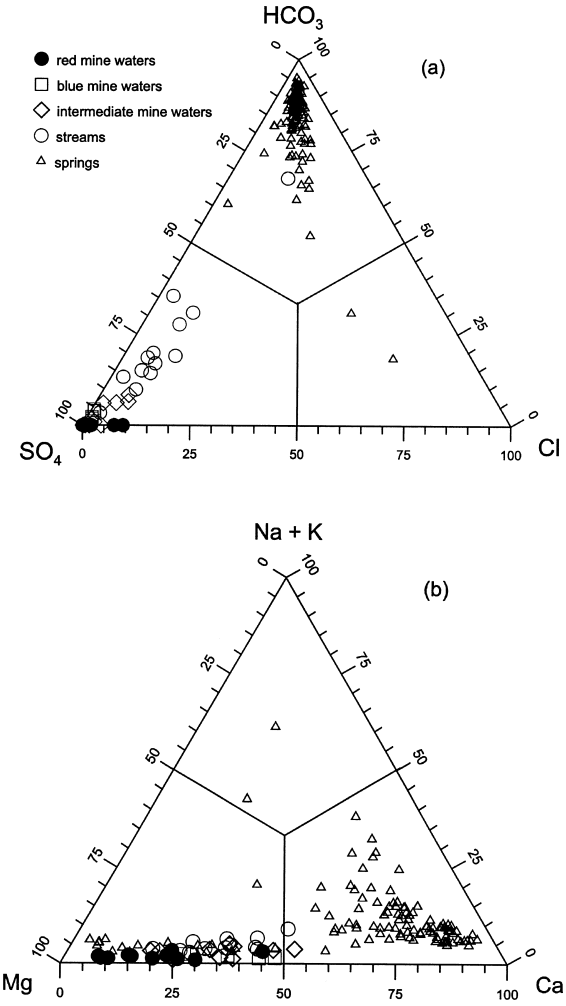

Fig. 3. (a) Relative Cl, SO_4 and HCO_3 concentrations and (b) relative Na + K, Ca and Mg contents, both in equivalent units, for the waters of the study area.

3b), both in equivalent units. Inspection of these plots shows that the composition of spring waters varies from Ca-HCO_3 to Mg-HCO_3, apart from two Na-Cl springs, which are located near the coast and are affected by seawater intrusion. Based on the geographical distribution of these Ca- and Mg-rich waters and the geology of the investigated area, it seems likely that Ca-HCO_3 waters are generated by dissolution of calcite-bearing sedimentary rocks, while Mg-HCO_3 waters are originated by leaching of serpentinites (Bruni *et al.*, 2002). Springs with characteristics intermediate between those of Ca-HCO_3 and Mg-HCO_3 waters are produced by interaction with gabbros and basalts. Magnesium and SO_4 are the prevailing cation and anion, respectively, in both the mine waters and the river waters downstream of the mine discharges. The abundance of SO_4 is evidently due to oxidative dissolution of pyrite, whereas the dominance of Mg reflects dissolution of serpentinites and other ophiolitic rocks.

MINE WATERS

Two distinct groups of waters are found at Libiola, the red waters and the blue waters, whose names reflect the color of the solid phases deposited (see below). Red waters have low pH (2.4–2.8) and high Eh (~600 mV) whereas blue waters have close to neutral pH (6.4–7.5) and lower Eh values (60–355 mV). Red waters have very high concentrations of sulfate (3500–9600 ppm) and dissolved metals, especially Fe (100–1000 ppm), Al (20–200 ppm), Cu (20–180 ppm), and Zn (20–50 ppm). Blue waters are poorer in metals than red waters, and sulfate attains 1400–2200 ppm.

Red waters are discharged by the two longest and lowest tunnels, called Ida and Castagna, whereas blue waters emerge from the third longest gallery, named Margherita. Adits of the Ida and Castagna tunnels are located in the bottom of the Gromolo valley, at 106.5 and 72.4 m above msl, respectively. The entrance of the Margherita gallery is at 209 m above msl near the Rio Cattan, a tributary of the Rio Gromolo (Fig. 2). All these sites have rather constant flowrate throughout the year (Dinelli *et al.*, 2001), consistent with their location close to the intersection of the water table with the topographic surface.

Some water discharges located at higher altitudes in the mine area are strongly affected by fluctuations of the water table, others are fed by ephemeral perched circuits and are active after the rainy periods only. They exhibit remarkable changes in physical and chemical characteristics with time (Dinelli *et al.*, 2001). For example, a pH variation from 3.8 to 6.2, accompanied by a marked decrease in dissolved Fe, Cu, and Al and

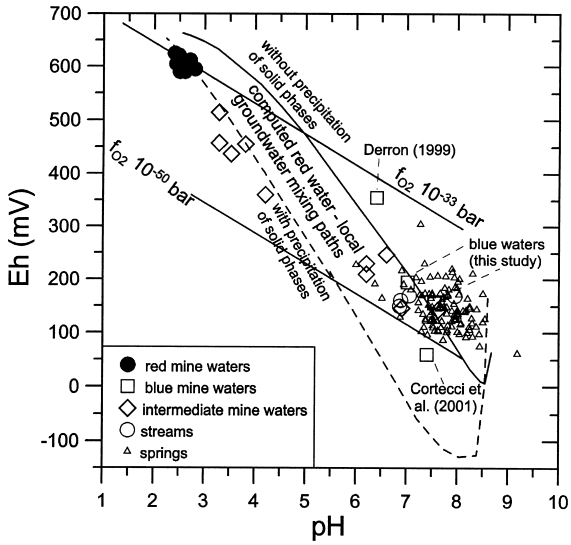

Fig. 4. Eh-pH plot for the waters of the study area.

by a change in color of the solid precipitates, from red to blue, was observed for one of these water emissions (Dinelli and Tateo, 2002). These water discharges are termed intermediate mine waters in the following discussion.

This distinction is substantiated by the Eh-pH plot (Fig. 4), in which most intermediate waters plot between the red waters and the blue waters. The latter two groups constitute two well defined clusters, characterized by little changes in Eh and pH. Eh and pH values of red and blue waters average f_{O_2} of ~10^{-33} bar and ~10^{-45} bar, respectively. The redox conditions of blue waters are comparable with those of the spring waters collected in unmined parts of the study area, whose lower f_{O_2} limit is close to 10^{-50} bar.

SOLID PHASES PRECIPITATED BY MINE WATERS

Amorphous silica, Fe(III) oxyhydroxides, schwertmannite, and less frequently jarosite were identified among the solid phases precipitated by the red waters (Dinelli *et al.*, 1998; Derron, 1999; Dinelli and Tateo, 2002).

According to Derron (1999), an Al hydroxisulfate (probably basaluminite), an Al hydroxide (gibbsite), amorphous silica, and a sulfate hydrate constitute the precipitates of the blue waters. The blue color of these precipitates is due to the presence of a Cu compound, which might be a Cu-Al sulfate hydrate of the woodwardite group [$(Cu,Al)_8SO_4(OH)_{16}\cdot nH_2O$]. On the other hand, according to Dinelli and Tateo (2002), no mineral phases can be identified in the blue water precipitates, due to their very poor crystallinity. The prevalent chemical constituents in these solids are Cu, volatiles, Al, and Si. Basaluminite was instead detected by Dinelli and Tateo (2002) in the whitish sediments of the Rio Boeno, some 100 m downstream of the mine waste area, where water pH is ~5.

Further hints on the product solid phases possibly deposited by mine waters are provided by the thermodynamic affinities to equilibrium with respect to relevant minerals, which were computed by means of the computer code EQ3NR (Wolery, 1992; see Table 2, where the chemical formulae of secondary minerals quoted in the text are also reported). Red waters are slightly oversaturated with respect to jurbanite and strongly undersaturated with gibbsite and basaluminite, whereas the opposite is true for blue waters, which are close to saturation with respect to gibbsite and basaluminite and undersaturated with jurbanite. These indications agree with the analytical results for the solid phases precipitated by blue waters, as well as with the findings of Nordstrom (1982b), who showed that the concentration of dissolved Al, at pH lower than ~4.6 and high sulfate concentrations, is usually constrained by saturation with respect to Al-sulfate-(hydroxyl) solid phases, such as jurbanite, alunite, and alunogen, whereas above pH 4.6 the less soluble phases gibbsite and/or basaluminite govern Al solubility.

Table 2 also indicates, consistently with the analytical results on solid phases, that (1) both red and blue waters are close to saturation with amorphous silica, (2) red waters are close to saturation with jarosite and natrojarosite, wheras blue waters are strongly undersaturated with these phases, and (3) red waters are close to saturation with Fe(III) hydroxide and schwertmannite, whereas blue waters appear to be oversaturated with re-

Table 2. Thermodynamic affinities to equilibrium with respect to relevant minerals (kcal/mol) for a red water (sample 168) and a blu water (sample 154). P_{CO_2} was assumed to be equal to $10^{-3.5}$ bar for sample 168.

Mineral	Formula	red 168	blu 154
Alunite	$KAl_3(SO_4)_2(OH)_6$	–8.86	–4.53
Alunogen	$Al_2(SO_4)_3 \cdot 17H_2O$	–9.64	–35.4
Antlerite	$Cu_3SO_4(OH)_4$	–12.8	0.383
Basaluminite	$Al_4SO_4(OH)_{10} \cdot 5H_2O$	–21.6	–3.23
Brochantite	$Cu_4SO_4(OH)_6$	–20.5	1.92
Calcite	$CaCO_3$	–15.0	–0.205
Chrysocolla	$CuSiH_4O_5$	–9.07	–0.576
Epsomite	$MgSO_4 \cdot 7H_2O$	–3.06	–4.10
Fe(III) hydroxide	$Fe(OH)_3$	–1.60	2.98
Gibbsite	$Al(OH)_3$	–6.36	1.75
Gypsum	$CaSO_4 \cdot 2H_2O$	–0.511	–0.659
Hydromagnesite	$Mg_5(CO_3)_4(OH)_2.4H_2O$	–84.0	–15.7
Jarosite	$KFe_3(SO_4)_2(OH)_6$	–0.588	–6.64
Jarosite-Na	$NaFe_3(SO_4)_2(OH)_6$	–1.27	–9.18
Jurbanite	$AlSO_4OH \cdot 5H_2O$	1.20	–4.80
Malachite	$Cu_2CO_3(OH)_2$	–18.2	0.881
Melanterite	$FeSO_4 \cdot 7H_2O$	–2.57	–7.95
Mn(II) sulfate	$MnSO_4$	–12.5	–14.0
Pyrite	FeS_2	–148.0	–111.0
Rhodochrosite	$MnCO_3$	–14.3	–0.924
Saponite-Ca	$Ca_{0.165}Mg_3Al_{0.33}Si_{3.67}O_{10}(OH)_2$	–35.8	5.92
Saponite-Mg	$Mg_{3.165}Al_{0.33}Si_{3.67}O_{10}(OH)_2$	–35.6	5.98
Schwertmannite	$Fe_8O_8(OH)_{4.5}(SO_4)_{1.75}$	1.12	13.3
Siderite	$FeCO_3$	–11.7	–2.12
Smithsonite	$ZnCO_3$	–13.9	–0.965
Amorphous silica	SiO_2	0.357	–0.235
Zn sulfate epta hydrate	$ZnSO_4 \cdot 7H_2O$	–4.56	–6.57

spect to both Fe(III) hydroxide and schwertmannite. However, most iron "dissolved" in blue waters might actually be very fine particulate as observed in many natural waters (Langmuir, 1997).

Red waters are undersaturated with respect to the Cu hydroxy-sulfates antlerite and brochantite, but blue waters attain saturation with these phases, which could be responsible for the color of the deposits accompanying these waters. Both red and blue waters are close to saturation with gypsum but undersaturated with respect to epsomite, melanterite, $ZnSO_4 \cdot 7H_2O$, and $MnSO_4$. Therefore the sulfate hydrate deposited by blue waters (see above) is most likely gypsum. As expected, all mine waters are strongly undersaturated with pyrite, which can be dissolved by all these aqueous solutions.

Reaction Path Modeling of Water-Rock Interaction and Mixing

To understand the importance of the processes that might govern the chemistry of Libiola mine waters, the irreversible mass exchanges taking place during both water-rock interaction and mixing between acid mine waters and local groundwaters were simulated by means of the software package EQ3/6, version 7.2b (Wolery, 1979, 1992; Wolery and Daveler, 1992).

Reference was made to the COM thermodynamic database, which lists the thermodynamic properties of many solids, aqueous species, and gases, mostly derived from SUPCRT92 (Johnson *et al.*, 1992). However, the solubility products of basaluminite, jurbanite (Nordstrom, 1982b), $CuCO_3$ (Sverjensky, 1984), $Cu(OH)_2$ (Marini *et*

al., 2001), and schwertmannite were also included in the thermodynamic database. For the latter mineral, the following hydrolysis reaction:

$$Fe_8O_8(OH)_{4.5}(SO_4)_{1.75} + 20.5H^+ = 8Fe^{3+} + 1.75SO_4^{2-} + 12.5H_2O \quad (1)$$

was considered, taking a log*K* of 8.0, which is the lowest value suggested by Yu *et al*. (1999). This choice and the alternative adoption of the uppermost log*K* proposed by the same authors, 13.0, will be discussed below.

Based on field evidence, analyses of solid phases, and thermodynamic affinities to equilibrium with respect to relevant minerals for mine waters (see above), the following pure solid phases were allowed to precipitate during both water-rock interaction and mixing between acid mine waters and local groundwaters: alunite, amorphous silica, antlerite, basaluminite, brochantite, chrysocolla, epsomite, gypsum, jarosite, Na-jarosite, jurbanite, melanterite, $MnSO_4$, schwertmannite, $ZnSO_4{\cdot}7H_2O$. For the same reasons, the separation of the following ideal solid mixtures* was allowed also: (1) a solid mixture of trigonal carbonates including calcite, siderite, rhodochrosite, smithsonite, and Cu-carbonate; (2) a solid mixture of the hydroxides of Fe(III), Fe(II), Mn(III), Mn(II), Zn, and Cu(II); (3) a saponite solid mixture comprising the Mg, Ca, Na, K, Fe(III), Fe(II), Mn(III), and Mn(II) endmembers. The thermodynamic data of the saponites of transition metals were estimated by Fantoni *et al*. (2002) following Sverjensky (1984, 1985). Ideal mixing was assumed since this is the only solid mixing model supported by version 7.2b of the EQ3/6 software package.

Water-rock interaction

Reaction path modeling was carried out in reaction progress mode, assuming bulk dissolution of the solid reactant, i.e., without any constraint on the mineralogy and dissolution rates of primary solid phases. At each step of the reaction progress variable, ξ, a corresponding amount of the solid reactant is added to the considered system, which is made up of the aqueous solution and possible product phases. The added reactant is dissolved instantaneously and resulting product phases, if any, are re-equilibrated immediately with the aqueous solution (Wolery and Daveler, 1992).

Simulation was carried out in two steps, at constant temperature, 15°C, P_{CO_2}, $10^{-3.5}$ bar, and f_{O_2}, 10^{-33} bar (and 10^{-50} bar in a separate run) in order to reproduce the range of temperature-pH-redox conditions of the environment under investigation. In Fig. 4 computed pH and Eh fall along the two lines labelled "f_{O_2} 10^{-33} bar" and "f_{O_2} 10^{-50} bar", also encompassing all the available analytical data.

In the first step, the average meteoric water of coastal regions (Berner and Berner, 1996; Bruni *et al*., 2002) was reacted, in two separate runs, with either 160 mmoles (6400 mg) or 3.33 mmoles (133 mg) of stoichiometric pyrite to span the range of dissolved SO_4 concentration. A hydroxide solid mixture, made up of almost pure $Fe(OH)_3$, and schwertmannite were the only solid phases produced during this first step of the simulation. Iron(III) hydroxide was generated above pH 4.3 and was replaced by schwertmannite below this pH value.

In the second step the acidic aqueous solution obtained through pyrite dissolution was reacted with a local mine-spoil material, sample Lb7, whose composition is given in Table 3. The neutralization of the aqueous solution previously produced through dissolution of 6400 mg of stoichiometric pyrite, under an f_{O_2} of 10^{-33} bar, brings about the precipitation of (in order of appearance) amorphous SiO_2, jarosite, jurbanite, schwertmannite, antlerite, alunite, a solid mixture of hydroxides (mostly $Fe(OH)_3$), gypsum, basaluminite, brochantite, and a saponite solid mixture (mainly Mg- and Ca-endmembers) (Fig. 5). Jarosite, jurbanite, schwertmannite, and antlerite have ephemeral existence and are re-

**The term "solid solution" is generally preferred to "solid mixture" in the geochemical literature. However in a solution it is possible to distinguish the solvent from the solute(s), which is not the case for the "solid solutions". These should be called, therefore, "solid mixtures".*

Table 3. Composition of the mine-spoil material Lb7 used as solid reactant in reaction path modeling

Constituent		Concentration
SiO_2	(wt%)	39.81
Al_2O_3	(wt%)	5.42
FeO	(wt%)	21.91
MnO	(wt%)	0.07
MgO	(wt%)	14.11
CaO	(wt%)	3.46
Na_2O	(wt%)	0.30
K_2O	(wt%)	0.06
C	(wt%)	0.14
S	(wt%)	0.54
LOI	(wt%)	11.8
Cu	(ppm)	1550
Zn	(ppm)	56.6

placed, at relatively high values of ξ, by alunite, basaluminite, the hydroxide solid mixture, and brochantite, respectively.

During the neutralization of the aqueous solution previously generated through dissolution of 133 mg of pyrite, under an f_{O_2} of 10^{-33} bar, jarosite, gypsum, antlerite, and brochantite are not generated (as well as schwertmannite under an f_{O_2} of 10^{-50} bar), but a carbonate solid mixture (chiefly calcite with subordinate rhodochrosite) is precipitated at comparatively high values of ξ.

These differences indicate the extreme sensitivity of the reaction path model to partial changes in the externally imposed conditions. Of course, in natural systems the generation of acidic aqueous solutions through oxidative dissolution of pyrite and the (partial) neutralization of these aqueous solutions through rock titration proceed simultaneously rather than in two distinct steps as hypothesized in our simulation. However, our approach is justified by the different kinetics of the two steps, with pyrite dissolution proceeding much faster than dissolution of silicate minerals.

As expected, acidity, total SO_4 and total Fe concentrations increase with the amount of pyrite consumed in the first step of the simulation. The aqueous solutions produced through oxidative dissolution of pyrite are characterized by the presence of an effective pH-buffer made up of the sulfate/bisulfate couple, whose iso-activity pH (where the buffer capacity is highest) is 1.87 at 15°C. Consequently, in the second step of the simulation, pH varies slowly with ξ, at least until "all" the bisulfate ion has been converted into sulfate ion (Fig. 6). Further rock dissolution brings about a sharp pH increment, since no effective buffers are present in the intermediate pH region. Weak buffering effects are due to the coexistence

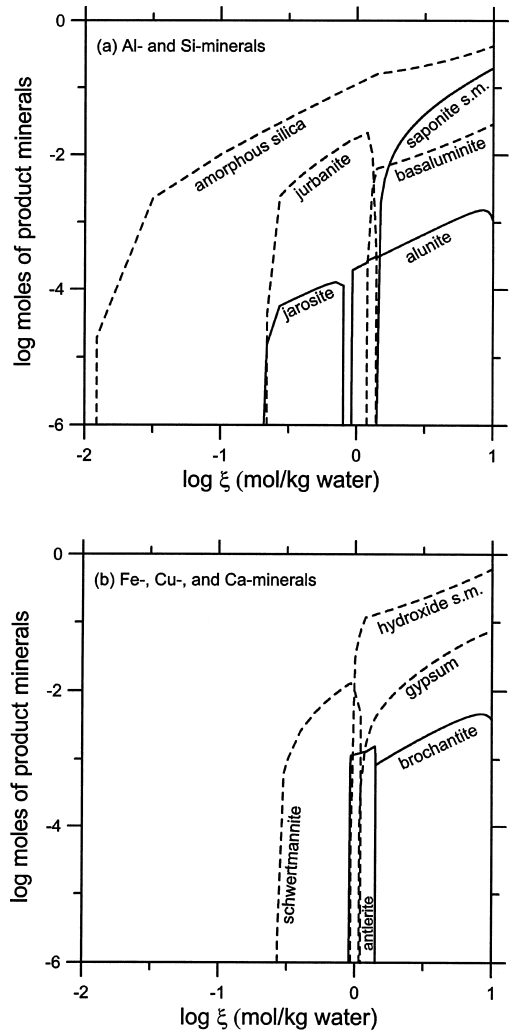

Fig. 5. Moles of mineral phases produced through progressive neutralization of the aqueous solution previously produced by dissolution of 6400 mg of stoichiometric pyrite, at f_{O_2} of 10^{-33} bar, temperature of 15 °C, and P_{CO_2} of $10^{-3.5}$ bar; s.m. = solid mixture.

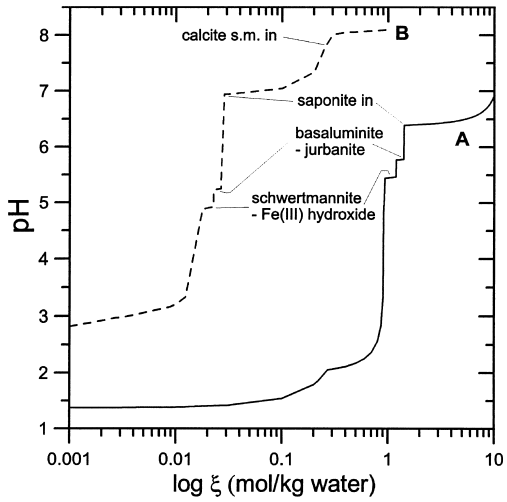

Fig. 6. Rock titration curves of the aqueous solution, previously produced through dissolution of (A) 6400 mg and (B) 133 mg of stoichiometric pyrite, at f_{O_2} of 10^{-33} bar, temperature of 15 °C, and P_{CO_2} of $10^{-3.5}$ bar; s.m. = solid mixture.

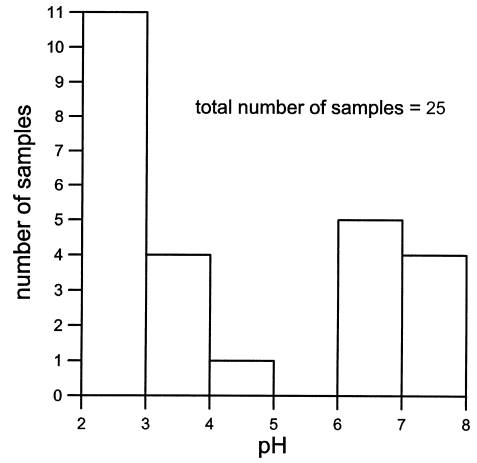

Fig. 7. Frequency distribution of pH of Libiola mine waters.

of the aqueous solution with schwertmannite-Fe(III) hydroxide first and jurbanite-basaluminite later on, whereas the simultaneous presence of antlerite and brochantite has a totally negligible buffering effect. Attainment of saturation with respect to either saponites or carbonates represents, instead, an effective pH-buffer, a condition shared with most natural waters, but this state is reached only at pH close to 6.5–7.0. The lack of intermediate pH buffers between the sulfate/bisulfate buffer and either the carbonate buffer or the saponite buffer explains the bimodal pH distribution for the twenty-five waters of the Libiola mine area (Fig. 7). A similar, bimodal frequency distribution was also observed for the pH of coalfields waters in Pennsylvania and the pH of volcanic lakes. The coal-mine drainage in Pennsylvania has an acidic mode at pH 2.5 to 4 and a near neutral mode at pH 6 to 7 with few samples having pH 4.5 to 5.5 (Cravotta *et al.*, 1999). Volcanic lake waters (220 entries) have bimodal pH distribution with an acidic mode at pH 0.5 to 1.5 and a near neutral mode at pH 6 to 6.5 with very few samples having pH 3.5 to 5 (Marini *et al.*, 2003).

Mixing of acid mine waters and local groundwaters

This process was simulated by mixing sample 168, a red water with 9000 ppm SO_4 and pH 2.5, with spring 106, which is situated near the Libiola mine area but has close to background values of dissolved constituents. Two separate runs were performed, either allowing or preventing the precipitation of product solid phases. Again, the simulation was carried out at temperature of 15°C and P_{CO_2} of $10^{-3.5}$ bar, but no constraint was set on f_{O_2}. In Fig. 4, calculated Eh and pH define two paths which are much steeper than those of water-rock interaction, but are also consistent with most analytical data. Only in the high pH region (low fractions of acid mine water) is the Eh computed admitting precipitation of solid phases somewhat lower than expected.

The main precipitated minerals include the carbonate solid mixture (chiefly calcite and siderite), the saponite solid mixture (mainly Mg- and Ca-components), the hydroxide solid mixture (mostly Fe(III) hydroxide), and basaluminite for fractions of acid water lower than 0.1–0.15, whereas jurbanite, schwertmannite, and amorphous silica are produced above this threshold (Fig. 8). Alunite and antlerite have a limited importance.

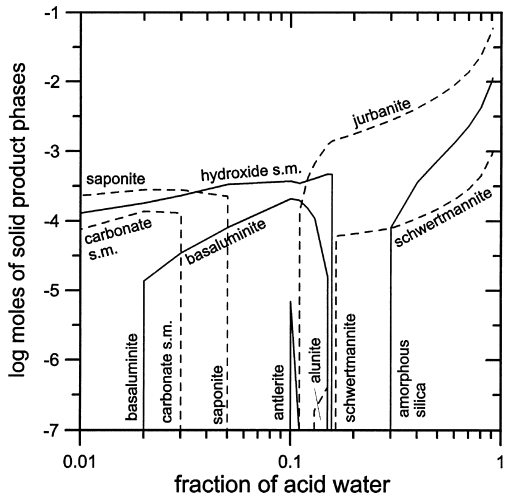

Fig. 8. Moles of mineral phases produced during mixing of the acid mine water 168 and the local groundwater 106 at temperature of 15°C and P_{CO_2} of $10^{-3.5}$ bar; s.m. = solid mixture.

DISCUSSION

Results of reaction path modeling for both water-rock interaction and mixing between acid mine waters and local groundwaters are plotted in suitable activity plots (Figs. 9–12), also reporting the analytical data of Libiola mine waters and nearby surface waters and groundwaters.

Activity plots are used as they represent the best tools to investigate mineral-solution equilibria (Helgeson, 1968). Since the alteration mineralogy prevailing in mine areas is dominated by sulfate and hydroxide minerals, the fields of stability of these phases are shown in the activity plots of Figs. 9–12 together with those of relevant carbonates. In each of these diagrams the $\log(a_{Me^{n+}})/(a_{H^+})^n$ ratio (where Me^{n+} stands for a generic cation of charge n^+) is plotted against the $\log(a_{SO_4^{2-}}) \times (a_{H^+})^2$ product.

All mine waters have $\log(a_{SO_4^{2-}}) \times (a_{H^+})^2$ product higher than those of local groundwaters whereas the $\log(a_{Me^{n+}})/(a_{H^+})^n$ ratios of acid mine waters are lower than those of local groundwaters. Therefore trends with negative slopes are observed in all these diagrams.

Red waters plot close to the neutralization path of the aqueous solution obtained through dissolution of 6400 mg of stoichiometric pyrite, indicating that their origin is satisfactorily explained by water-rock interaction and there is no need to invoke occurrence of mixing with local groundwaters.

In the activity plots for the MgO-SO_3-CO_2-H_2O system (Fig. 9a), the CaO-SO_3-CO_2-H_2O system (Fig. 9b), the CuO-SO_3-CO_2-H_2O system (Fig. 10a), the ZnO-SO_3-CO_2-H_2O system (Fig. 10b), the MnO-SO_3-CO_2-H_2O system (Fig. 11a), and the Al_2O_3-SO_3-H_2O system (Fig. 11b) the blue waters and some intermediate waters are located between the different neutralization paths and close to the mixing lines, suggesting that both water-rock interaction and mixing might be responsible of the origin of these water discharges. However, the intermediate waters 53, 8apr, and 12apr are situated relatively far from the mixing lines and close to the neutralization path of the aqueous solution generated through dissolution of 133 mg of stoichiometric pyrite. This fact is particularly evident in the activity plots for the ZnO-SO_3-CO_2-H_2O system (Fig. 10b) and the MnO-SO_3-CO_2-H_2O system (Fig. 11a), indicating that water-rock interaction is probably more apt than mixing to explain the origin of these samples. Alternatively, the spread of analytical data in these plots could be ascribed, at least partly, to the involvement of mine-spoil materials with metal contents different from those of the considered solid reactant, i.e., sample Lb7. For instance, in the activity plot for the CuO-SO_3-CO_2-H_2O system (Fig. 10a), samples 53, 8apr, and 12apr have $\log(a_{Cu^{2+}})/(a_{H^+})^2$ ratios even lower than those of the neutralization path of the aqueous solution generated through dissolution of 133 mg of stoichiometric pyrite, independent of redox conditions, suggesting that a mine-spoil material poorer in Cu than sample Lb7 is probably involved in their origin.

The comparison between theoretical paths and analytical data in the activity plots for the Fe_2O_3-SO_3-H_2O system (Fig. 12a) and the FeO-SO_3-CO_2-H_2O system (Fig. 12b) suggests that mixing with or without precipitation of solid phases (based on Fe^{2+}) or at least mixing without precipitation of

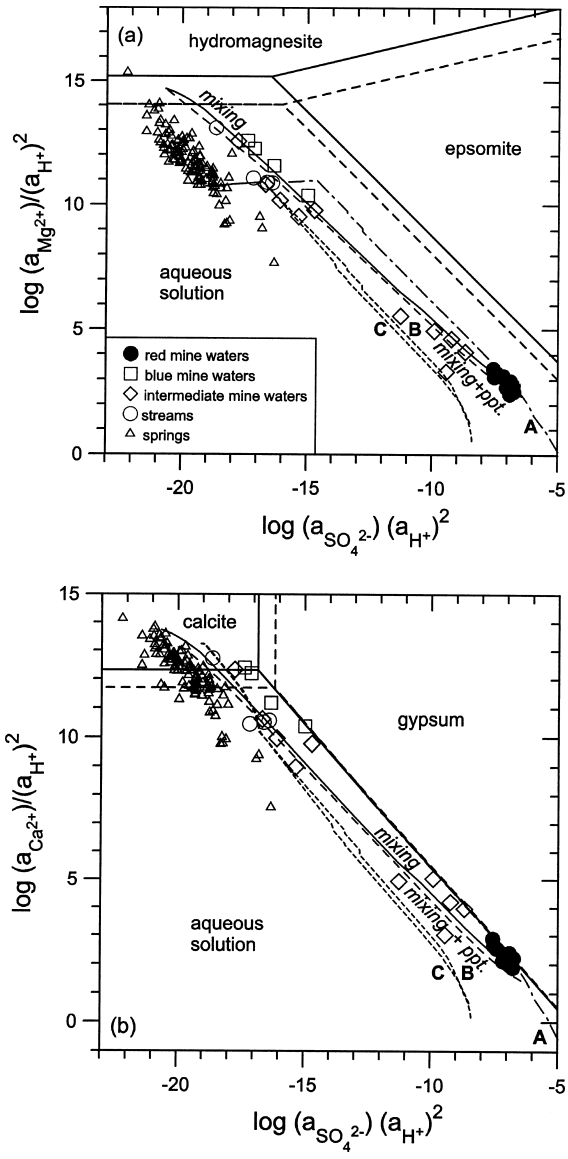

Fig. 9. Activity plots for (a) the MgO-SO_3-CO_2-H_2O system and (b) the CaO-SO_3-CO_2-H_2O system. Phase stability limits refer to the temperature of 0°C (solid line) and 25°C (dashed line). Also shown are the theoretical trends for neutralization of acid aqueous solutions produced by oxidative dissolution of (A) 6400 mg of pyrite and (B, C) 133 mg of pyrite, as well as the computed paths for mixing of red water 168 and local groundwater 106, with precipitation of solid phases (dashed line) or without it (solid line), all at temperature of 15°C and P_{CO_2} of $10^{-3.5}$ bar. Paths A and B refer to f_{O_2} of 10^{-33} bar while path C is computed for f_{O_2} of 10^{-50} bar.

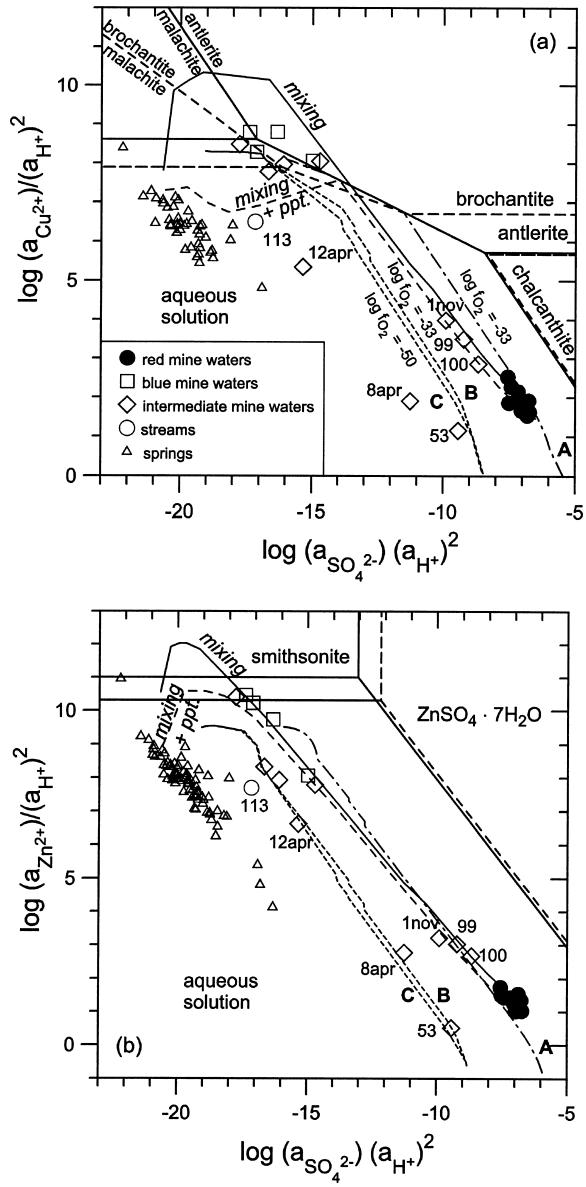

Fig. 10. Activity plots for (a) the CuO-SO_3-CO_2-H_2O system and (b) the ZnO-SO_3-CO_2-H_2O system. Phase stability limits refer to the temperature of 0°C (solid line) and 25°C (dashed line). Also shown are the theoretical trends for neutralization of acid aqueous solutions produced by oxidative dissolution of (A) 6400 mg of pyrite and (B, C) 133 mg of pyrite, as well as the computed paths for mixing of red water 168 and local groundwater 106, with precipitation of solid phases (dashed line) or without it (solid line), all at temperature of 15°C and P_{CO_2} of $10^{-3.5}$ bar. Paths A and B refer to f_{O_2} of 10^{-33} bar while path C is computed for f_{O_2} of 10^{-50} bar.

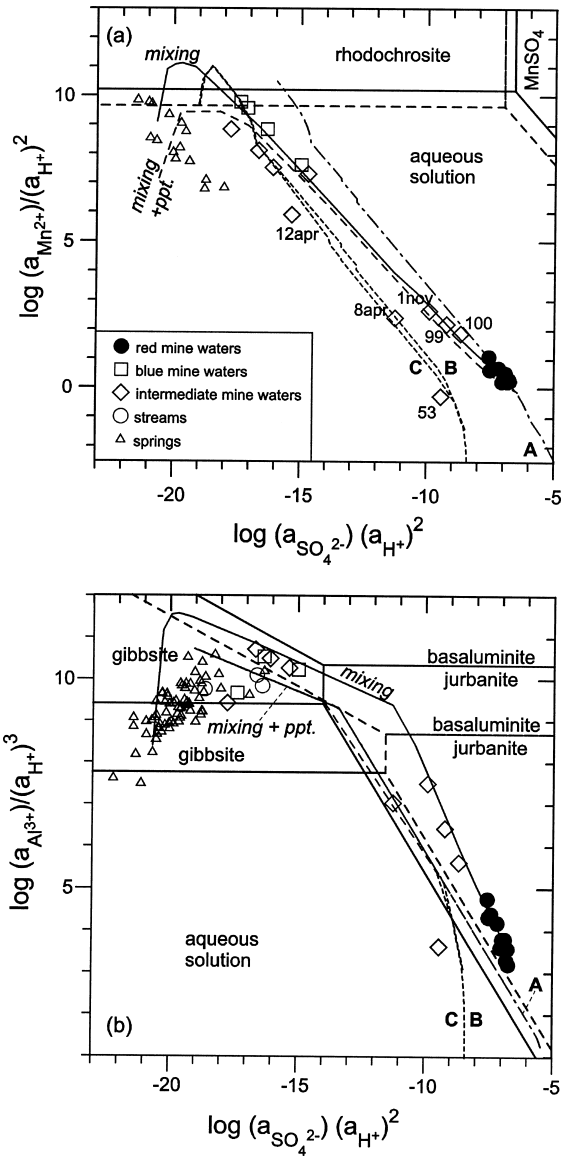

Fig. 11. Activity plots for (a) the MnO-SO_3-CO_2-H_2O system and (b) the Al_2O_3-SO_3-H_2O system. Phase stability limits refer to the temperature of 0°C (solid line) and 25°C (dashed line). Also shown are the theoretical trends for neutralization of acid aqueous solutions produced by oxidative dissolution of (A) 6400 mg of pyrite and (B, C) 133 mg of pyrite, as well as the computed paths for mixing of red water 168 and local groundwater 106, with precipitation of solid phases (dashed line) or without it (solid line), all at temperature of 15°C and P_{CO_2} of $10^{-3.5}$ bar. Paths A and B refer to f_{O_2} of 10^{-33} bar while path C is computed for f_{O_2} of 10^{-50} bar.

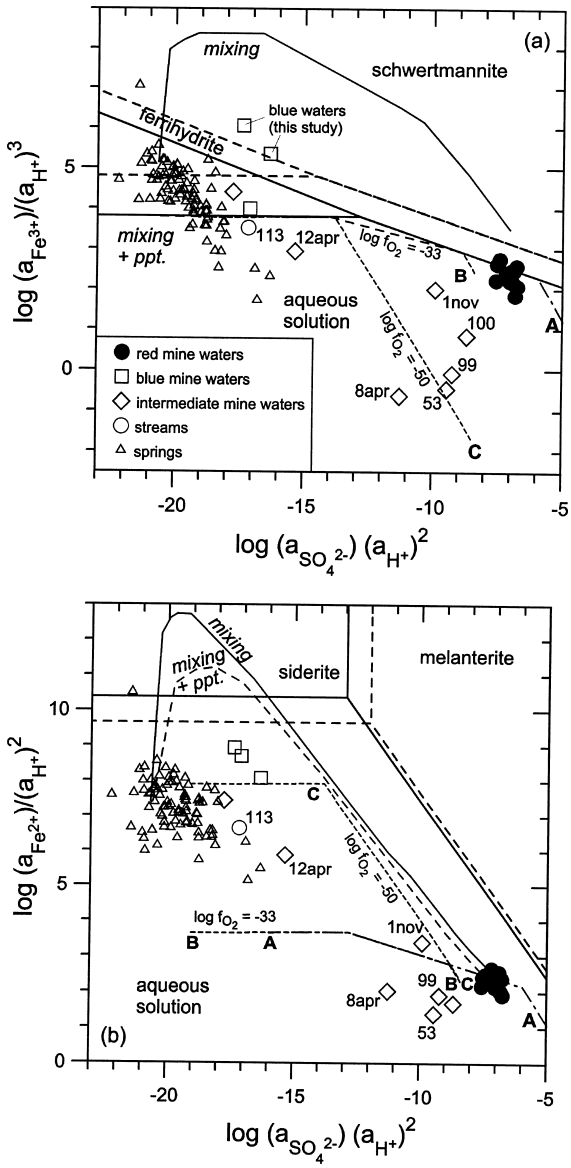

Fig. 12. Activity plots for (a) the Fe_2O_3-SO_3-H_2O system and (b) the FeO-SO_3-CO_2-H_2O system. In (a) phase stability limits refer to $\log K_{schwertmannite}$ of 8.0 (solid line) and 13.0 (dashed line), but in (b) phase stability limits refer to the temperature of 0°C (solid line) and 25°C (dashed line). Also shown are the theoretical trends for neutralization of acid aqueous solutions produced by oxidative dissolution of (A) 6400 mg of pyrite and (B, C) 133 mg of pyrite, as well as the computed paths for mixing of red water 168 and local groundwater 106, with precipitation of solid phases (dashed line) or without it (solid line), all at temperature of 15°C and P_{CO_2} of $10^{-3.5}$ bar. Paths A and B refer to f_{O_2} of 10^{-33} bar while path C is computed for f_{O_2} of 10^{-50} bar.

solid products (based on Fe^{3+}) are unlikely to govern the characteristics of blue waters and intermediate waters.

In principle, this conclusion could be biased by uncertainties in the solubility product of schwertmannite. As already recalled, the lowest log*K* value proposed by Yu *et al*. (1999), 8.0, was inserted in the thermodynamic database of the software package EQ3/6, but the theoretical grid for log*K* of 13.0, the uppermost value suggested by the same authors, is also reported in the activity plot of Fig. 12a. If this value were adopted, the water-rock interaction paths and the mixing line with precipitation of solid phases would shift towards higher $\log(a_{Fe^{3+}})/(a_{H^+})^3$ ratios, but the picture would remain basically the same. Much higher log*K* values, 18 ± 2.5, were indicated for schwertmannite by Bigham *et al.* (1996). However, if this solubility window is adopted, all the red waters of Libiola are strongly undersaturated with respect to schwertmannite, which is considered unlikely based on the findings by Dinelli and Tateo (2002). Therefore, the indication provided by the activity plot for the Fe_2O_3-SO_3-H_2O system (Fig. 12a) is considered to be right, i.e., the characteristics of blue waters and intermediate waters are not controlled by mixing without precipitation of solid products.

For the activity plot for the FeO-SO_3-CO_2-H_2O system (Fig. 12b), one could object that the "analytical" data are not totally reliable, as they were computed through the speciation code EQ3NR, starting from concentrations of total dissolved Fe and Eh values. Although this is not an error-free way to obtain the concentrations of dissolved Fe(III) and Fe(II), Eh measurements are usually reliable in Fe-rich acid mine waters, as demonstrated by the excellent agreement between computed and measured Eh values (Nordstrom *et al*., 1979). On the other hand, measurement of Fe(II) and total Fe and computation of Fe(III) by difference is likely to bring about large uncertainties in the Fe(III) data, considering that computed concentrations of dissolved Fe(III) and Fe(II) in sample 168 are 0.23 and 14.9 mmol/kg, respectively. Assuming that Fe^{2+} "analytical" data are good enough, the suggestion provided by the activity plot for the FeO-SO_3-CO_2-H_2O system (Fig. 12b) is considered to be correct, i.e., the features of blue waters and intermediate waters are not governed by mixing, with or without precipitation of solid products.

Summing up, we conclude that the main process governing the chemical characteristics of all the mine waters of Libiola, red, blue, and intermediate, is variable interaction with mine-waste materials. Mixing between acid mine waters and local groundwaters plays a subordinate role, if any.

CONCLUSIONS

Waters discharging from the mine area of Libiola can be distinguished as: (1) red waters, characterized by low pH (2.4–2.8), high Eh (~600 mV), and very high contents of sulfate and dissolved metals; (2) blue waters with neutral pH (7.0–7.5), Eh values of 60–355 mV, and concentrations of sulfate and dissolved metals lower than red waters; (3) waters with intermediate characteristics, that we have termed intermediate waters. Red and blue waters are discharged by the three longest and lowest elevation tunnels draining the mine area and have relatively stable physical and chemical characteristics throughout the year. Intermediate waters are found at higher elevations, are heavily influenced by fluctuations of the water table, and show strong variations in physical and chemical features with time (Dinelli *et al*., 2001).

The irreversible mass exchanges occurring during both interaction of meteoric waters with mine-spoil materials and mixing between acid mine waters and local groundwaters were simulated by means of the software package EQ3/6, to understand the role of these processes. Comparison of theoretical results with analytical data, carried out by means of suitable activity plots, suggests that the main process governing the chemistry of all the mine waters of Libiola is variable interaction of meteoric waters with mine tailings, while addition of local groundwaters to acid mine waters plays a minor role or is totally insignificant.

Based on computed data, a sharp pH change is expected in the intermediate pH region (roughly 3 to 6), during the neutralization of the acid aqueous solutions produced by oxidative dissolution of pyrite. This is due to the lack of effective pH buffers between the sulfate/bisulfate buffer (whose buffer capacity is highest at pH 1.87 for a temperature of 15°C) and the mineral buffers which are active in the neutral range. This explains the bimodal pH distribution in the mine waters of Libiola, similar to what was observed for coalfields waters of Pennsylvania (Cravotta *et al*., 1999) and volcanic lake waters (Marini *et al*., 2003).

Finally, it must be underscored that the acid waters discharged by the tunnels of the Libiola mine area enter the Rio Gromolo, determining a strong impact on this aqueous environment and posing a serious threat to the vegetal and animal biota. Precipitation of Fe(III) oxyhydroxide and amorphous Al phases (e.g., basaluminite) takes place upon mixing between acid mine waters and surface waters (Dinelli *et al*., 2001; Dinelli and Tateo, 2002) and most of these solid phases remain in suspension in river waters. Although precipitation of these minerals may scavenge some metals, river waters are heavily polluted, especially during the dry season, when their flowrate decreases. Investigation of these processes by means of reaction path modeling is under way at present and will be the subject of a separate communication.

REFERENCES

Abbate, E., Bortolotti, V., Galbiati, B. and Principi, G. (1980) *Carta geologica delle ofioliti del Borgonasco e dell'alta Val Graveglia*. L.A.C. Firenze.

Appelo, C. A. J. and Postma, D. (1996) *Geochemistry, Groundwaters and Pollution*. A.A. Balkema, Rotterdam, 536 pp.

Berner, E. K. and Berner, R. A. (1996) *Global Environment: Water, Air, and Geochemical Cycles*. Prentice Hall, Upper Saddle River, 376 pp.

Bertolani, M. (1952) I giacimenti cupriferi nelle ofioliti di Sestri Levante (Liguria). *Per. Min*. **21**, 149–170.

Bigham, J. M., Schwertmann, U., Traina, S. J., Winland, R. L. and Wolf, M. (1996) Schwertmannite and the chemical modeling of iron in acid sulfate waters. *Geochim. Cosmochim. Acta* **60**, 2111–2121.

Bonatti, E., Zerbi, M., Kay, R. and Rydell, H. (1976) Metalliferous deposits from the Apennine ophiolites: Mesozoic equivalents of modern deposits from oceanic spreading centers. *Geol. Soc. Am. Bull*. **87**, 83–94.

Brigo, L. and Ferrario, A. (1974) Le mineralizzazioni nelle ofioliti della Liguria Orientale. *Rend. S.I.M.P*. **30**, 305–316.

Bruni, J., Canepa, M., Cipolli, F., Marini, L., Ottonello, G., Vetuschi Zuccolini, M., Chiodini, G., Cioni, R. and Longinelli, A. (2002) Irreversible water-rock mass transfer accompanying the generation of the neutral, Mg-HCO_3 and high-pH, Ca-OH spring waters of the Genova province, Italy. *Appl. Geochem*. **17**, 455–474.

Cortecci, G., Dinelli, E., Lucchini, F. and Vaselli, O. (2001) Hydrogeochemical and isotopic investigations in the abandoned Fe-Cu mine of Libiola (northern Italy). *Proc. X WRI Conf*., Balkema, Rotterdam.

Cravotta, C. A., III, Brady, K. B. C., Rose, A. W. and Douds, J. B. (1999) Frequency distribution of the pH of coal-mine drainage in Pennsylvania. U.S. Geological Survey Toxic Substances Hydrology Program. Water Resources Investigation Report 99-4018A.

Decandia, F. A. and Elter, P. (1972) La zona ofiolitifera del Bracco nel settore compreso fra Levanto e la Val Graveglia (App. Ligure). *Mem. Soc. Geol. It*. **11**, 503–530.

Derron, M.-H. (1999) Interaction eau-roche de basse température: géochimie des métaux dans l'altèration météorique des roches mafiques alpine. Thése de doctorat. Faculté des Sciences de l'Université de Lausanne.

Dinelli, E. and Tateo, F. (2002) Different types of fine-grained sediments associated to acid mine drainage in the Libiola Fe-Cu mine area (Ligurian Apennines, Italy). *Appl. Geochem*. (in press).

Dinelli, E., Morandi, N. and Tateo, F. (1998) Fine-grained weathering products in waste disposal from two sulphide mines in the northern Apennines, Italy. *Clay Minerals* **33**, 423–433.

Dinelli, E., Lucchini, F., Fabbri, M. and Cortecci, G. (2001) Metal distribution and environmental problems related to sulfide oxidation in the Libiola copper mine area (Ligurian Apennines, Italy). *J. Geochem. Explor*. **74**, 141–152.

Dubuis, R., Moulin, C., Pfanzelter, A. and Roch, K. (1998) *Etude geochimique et isotopique des eaux des bassins versants Petronio & Gromolo*. Faculté des Sciences de l'Université de Lausanne, 151 pp.

Evangelou, V. P. (1995) *Pyrite Oxidation and Its Control*. CRC Press, 293 pp.

Fantoni, D., Brozzo, G., Canepa, M., Cipolli, F., Marini,

L., Ottonello, G. and Vetuschi Zuccolini, M. (2002) Natural hexavalent chromium in groundwaters interacting with ophiolitic rocks. *Environmental Geology* (submitted).

Ferrario, A. (1973) I giacimenti cupriferi delle pillow-lavas della Liguria Orientale. *Rend. S.I.M.P.* **29**, 485–495.

Ferrario, A. and Garuti, G. (1980) Copper deposits in the basal breccias and volcano-sedimentary sequences of the Eastern Ligurian Ophiolites (Italy). *Mineralium Deposita* **15**, 291–303.

Galli, M. and Penco, A. M. (1996) Le miniere di rame e di manganese della Liguria Orientale. *Atti dell'Accademia Ligure di Scienze e Lettere* **53**, 215–247.

Garrels, R. M. and Thompson, M. E. (1960) Oxidation of pyrite in iron sulfate solutions. *Am. J. Sci.* **258A**, 57–67

Helgeson, H. C. (1968) Evaluation of irreversible reactions in geochemical processes involving minerals and aqueous solutions: I. Thermodynamic relations. *Geochim. Cosmochim. Acta* **32**, 853–877.

Johnson, J. W., Oelkers, E. H. and Helgeson, H. C. (1992) SUPCRT 92: A software package for calculating the standard molal thermodynamic properties of minerals, gases, aqueous species, and reactions from 1 to 5000 bars and 0 to 1000°C. *Computers & Geosciences* **18**, 899–947.

Langmuir, D. (1997) *Aqueous Environmental Geochemistry*. Prentice Hall, Upper Saddle River, New Jersey, 600 pp.

Lowson, R. T. (1982) Aqueous oxidation of pyrite by molecular oxygen. *Chem. Rev.* **82**, 461–497.

Marini, L., Canepa, M., Cipolli, F., Ottonello, G. and Vetuschi Zuccolini, M. (2001) Use of stream sediment chemistry to predict trace element chemistry of groundwater. A case study from the Bisagno valley (Genoa, Italy). *J. Hydrol.* **241**, 194–220.

Marini, L., Vetuschi Zuccolini, M. and Saldi, G. (2003) The bimodal pH distribution of volcanic lake waters. *J. Volcanol. Geotherm. Res.* (in press).

McKibben, M. A. and Barnes, H. L. (1986) Oxidation of pyrite in low temperature acidic solutions: Rate laws and surface textures. *Geochim. Cosmochim. Acta* **50**, 1509–1520.

Moses, C. O. and Herman, J. S. (1991) Pyrite oxidation at circumneutral pH. *Geochim. Cosmochim. Acta* **55**, 471–482.

Moses, C. O., Nordsrom, D. K., Herman, J. S. and Mills, A. L. (1987) Aqueous pyrite oxidation by dissolved oxygen and ferric iron. *Geochim. Cosmochim. Acta* **51**, 1561–1572.

Nicholson, R. V., Gillham, R. W. and Reardon, E. J. (1988) Pyrite oxidation in carbonate buffered solution: 1. Experimental kinetics. *Geochim. Cosmochim. Acta* **52**, 1077–1085.

Nordstrom, D. K. (1977) Thermochemical redox equilibria of ZoBell's solution. *Geochim. Cosmochim. Acta* **41**, 1835–1841.

Nordstrom, D. K. (1982a) Aqueous pyrite oxidation and the consequent formation of secondary iron minerals. *Acid Sulphate Weathering* (Nordstrom, D. K., ed.), Soil Sci. Soc. Amer., Spec. Publ. **10**, 37–56.

Nordstrom, D. K. (1982b) The effect of sulfate on aluminum concentrations in natural waters: Some stability relations in the system Al_2O_3-SO_3-H_2O at 298 K. *Geochim. Cosmochim. Acta* **46**, 681–692.

Nordstrom, D. K., Jenne, E. A. and Ball, J. W. (1979) Redox equilibria of iron in acid mine waters. *Chemical Modeling of Aqueous Systems* (Jenne, E. A., ed.), 51–79, Am. Chem. Soc. Symp. Ser. 93, Washington, D.C.

Scott, S. (1997) Submarine hydrothermal systems and deposits. *Geochemistry of Hydrothermal Ore Deposits* (Barnes, H. L., ed.), 3rd ed., 797–875, Wiley, New York.

Singer, P. C. and Stumm, W. (1970) Acid mine drainage: The rate limiting step. *Science* **167**, 1121–1123.

Sverjensky, D. (1984) Prediction of Gibbs free energies of calcite-type carbonates and the equilibrium distribution of trace elements between carbonates and aqueous solutions. *Geochim. Cosmochim. Acta* **48**, 1127–1134.

Sverjensky, D. (1985) The distribution of divalent trace elements between sulfides, oxides, silicates and hydrothermal solutions. I. Thermodynamic basis. *Geochim. Cosmochim. Acta* **49**, 853–864.

Williamson, M. A. and Rimstidt, J. D. (1994) The kinetics and electrochemical rate-determining step of aqueous pyrite oxidation. *Geochim. Cosmochim. Acta* **58**, 5443–5454.

Wolery, T. J. (1979) Calculation of chemical equilibrium between aqueous solutions and minerals: the EQ3/6 software package. Report UCRL-52658, Lawrence Livermore National Laboratory, Livermore.

Wolery, T. J. (1992) EQ3NR, A computer program for geochemical aqueous speciation-solubility calculations: Theoretical manual, user's guide and related documentation (version 7.0). Report UCRL-MA-110662 PT III, Lawrence Livermore National Laboratory, Livermore.

Wolery, T. J. and Daveler, S. A. (1992) EQ6, A computer program for reaction path modeling of aqueous geochemical systems: Theoretical manual, user's guide, and related documentation (version 7.0). Report UCRL-MA-110662 PT IV, Lawrence Livermore National Laboratory, Livermore.

Yu, J.-Y., Heo, B., Choi, I.-K., Cho, J.-P. and Chang, H.-W. (1999) Apparent solubilities of schwertmannite and ferrihydrite in natural stream waters polluted by mine drainage. *Geochim. Cosmochim. Acta* **63**, 3407–3416.